Reduced friction and wear of electro-brush plated nickel composite coatings reinforced by graphene oxide

Qi, Shaojun; Li, Xiaoying; Dong, Hanshan

[Link to publication on Research at Birmingham portal](#)

Reduced friction and wear of electro-brush plated nickel composite coatings reinforced by graphene oxide

Shaojun Qi, Xiaoying Li, Hanshan Dong

School of Metallurgy and Materials, University of Birmingham, Birmingham B15 2TT, UK

Abstract

The nano-scale studies in the literature have revealed the excellent anti-friction properties of graphene and its great potential as a nano solid lubricant. However, for macro-scale applications the integrity and durability are main problems for most graphene-based surface coatings. One way to mediate the durability issue while exploiting the tribology of graphene is graphene-based composites. In this work, nickel-graphene oxide (GO) composite coatings were fabricated on steel by electro-brush plating. The effects of GO on the tribological properties were investigated. The results show that the composite coatings possess much lower friction than GO-free nickel coating (up to 47% less against a bearing steel ball, and 30% less against an alumina ball). As the GO load increases from 0 to 4 mg/ml, the wear rate of the resulting composite can be reduced significantly by approximately 90%. Detailed post-test studies of the wear tracks and the counterpart were conducted using SEM, EDS, Raman and FIB/SEM. The improved tribological properties can be attributed to the strengthening effect, the retention of oxide tribo-films and the formation of GO rolls during sliding. The tribological behaviour of the Ni-GO nano-composite coating and a Ni-graphite composite coating was compared, and their different wear mechanisms have been discussed.

Key words: Graphene oxide; Nano-composite coating; Friction and wear; Tribo-film; GO rolls

1. Introduction

Graphene has been deemed as a promising solid lubricant due to its proved extraordinary lubricity [1]. Early studies involving atomic force microscopy (AFM) and lateral force microscopy (LFM) on single to few-layer graphene have demonstrated that the coefficient of friction (COF) of graphene is similar or even superior to bulk graphite [2-4]. Considering the size effect (single-layer graphene measures ~0.34 nm thick), graphene and its derivatives possess great advantages over graphite a well-known engineering solid lubricant for nano and micro tribological applications. It has also been demonstrated that by

smart and delicate design of the graphene-surface contact, superlubricity (COF ~0.004) can be realised at macro scale [5]. Applying graphene and related materials as surface coatings to combat friction and wear in a common engineering context, however, is less reported due to the normally inadequate bonding between graphene and the substrate.

To exploit the tribological potential of graphene while addressing the durability issue with graphene surface coatings, recently a number of graphene-based composite coatings have been developed and their tribological properties reported [6-9]. Coating systems with metallic matrixes, such as TiAl [10], Cu [11, 12] and Ni [13, 14] have been reported. Among these, nickel matrix composite coatings are of particular interest due to the ease of fabrication and wide applications in engineering [8, 15]. Nickel matrix nano-composites have been prepared by conventional electroplating [16-18] or electroless deposition [19] techniques. Alternatively, an electro-brush plating (EBP) technique, which is widely used in the remanufacturing of work pieces [20, 21], can be adapted. However, no work on the brush-plating of nickel-graphene oxide composite coatings for tribological applications has been reported in the literature yet. A number of lubrication mechanisms of composites incorporating graphene and related materials have been reported. One of the most popular explanations is that the easy interlayer shear of the graphene species reduces the energy dissipation between the contact and thus reduces the friction [22, 23]. Other hypotheses include grain refinement effect [22], formation of low-friction carbon films [10, 24, 25], and synergistic lubricating effect of graphene and other nano particles [11, 26]. However, more comprehensive microstructural, mechanical and chemical investigations towards these proposed models are required.

In our previous study, nickel-graphene oxide nano-composite coatings were fabricated by EBP, and their mechanical properties and corrosion behaviour were evaluated [27]. In the present work, the tribological behaviour of the nickel-graphene oxide nano-composite coatings against different counter materials in air was investigated. To elucidate the difference between graphene oxide and graphite as the incorporation phase, a nickel-graphite composite coating was prepared and their tribological performance compared. Based on the experimental results and extensive post-test examination of the wear tracks and the counterpart surfaces, wear mechanisms for GO- and graphite-containing metallic-matrix composites were suggested.

2. Experimental

2.1. Coating fabrication

Graphene oxide (GO) was synthesised using graphite powder (Alfa Aesar, -325 mesh

natural flakes) via a modified Hummers' method and ultrasonication-assisted exfoliation as described elsewhere [27]. Type 316L stainless steel coupons were ground to grit 2500, cleaned and degreased before being used as the substrates. Commercially available (Sifco ASC, part No. 2086) nickel plating solution was used in this work. Composite plating solutions were prepared by adding concentrated GO suspension dropwise into the original plating solution under continuous ultrasonication (200 W) and vigorous shaking. Nickel-graphite plating solution was prepared in the same way but using graphite powder. Five types of plating solutions with varying GO/graphite incorporation were employed. The sample codes are listed in Table 1.

Table 1. Specification of the coatings

Incorporation load		GO			Graphite
(mg/ml)	0	0.5	2.0	4.0	4.0
Sample code	Ni	NG05	NG20	NG40	NGr40

The coatings were fabricated using a NBP-100 nano electro-brush plating unit where a plating brush wrapped with absorbent cotton cloth (i.e. anode) and the workpiece (i.e. cathode) were attached. During the plating process, the plating brush saturated with electrolyte wiped against the substrates with a constant pace of 10 cm/s and a voltage of 14 V over the substrate. after a plating time of 30 min, the resulting coatings were rinsed with deionised water and dried in hot air.

2.2. Microstructural characterisation

A Philips XL-30 field emission scanning electron microscope (FESEM) equipped with an energy dispersive X-ray spectroscope (EDS) was employed to examine the morphology and chemical compositions of the coatings. A confocal Raman microscope (Renishaw, 488 nm laser) was used to obtain characteristic spectra of the GO-containing coatings. The surface roughness of the coatings was measured on an Ambios XP-200 profilometer. Vickers hardness measurements were conducted using a Mitutoyo MVK-H1 micro-hardness tester. Nanoindentation measurements were performed on a NanoTest Vantage testing platform (Micro Materials Ltd.) fitted with a Berkovich indenter. The nano-hardness and Young's moduli were calculated from the loading-unloading curves based on a power law fit developed by Oliver and Pharr [28].

2.3. Tribological testing

Reciprocating wear tests were carried out in ambient air at room temperature on a ball-on-plate tribometer (TE79 multi-axis, Phoenix Tribology Ltd., UK). The samples

involved in the tribological study and the corresponding testing parameters are summarised in Table 2. Two different counter materials, chromium bearing steel balls (Spheric Trafalfar Ltd., GD 100, 700-900 Hv) and alumina balls (Spheric Trafalfar Ltd., 1700 Hv), both 8 mm in diameter, were used. The counter materials were selected to represent two potential engineering application situations where the coatings may be applied, i.e. metal-to-metal (coating *vs.* steel) and metal-to-ceramic (coating *vs.* alumina) contacts. The frictional behaviour of the tribo-pairs under varying normal loads at a frequency of 1 Hz, was observed. The worn surfaces were examined by SEM, EDS and a profilometer. The wear factor was calculated using the following equation:

$$k = \frac{V}{F \cdot s}$$ (1)

where V is the volume of material loss, F is the applied normal load, s is the total sliding distance, k is the wear factor in $mm^3 N^{-1} m^{-1}$. The wear loss volume was determined using the profilometer. The cross section of each wear track was scanned at no less than 3 different positions (typically left, middle and right). The wear volume was calculated by taking the mean value of the measured (3 or more) cross-sectional areas before multiplying the length of the wear track (which was 5 mm). In addition, observation of the GO rolls formed on the worn surfaces was performed using a dual beam FEI Quanta 3D FEG focused ion beam (FIB).

Table 2. Summary of the tribological testing parameters

| Counter material	Samples tested	Testing conditions		
		Load	Speed & frequency	Atmosphere
Bearing steel Φ 8 mm ball	Ni NG05, NG20, NG40 NGr40	1 N	5 mm/s, 1 Hz	Air
Alumina Φ 8 mm ball	Ni NG40 NGr40	1/3/5 N		

3. Results

3.1. Surface morphology and roughness
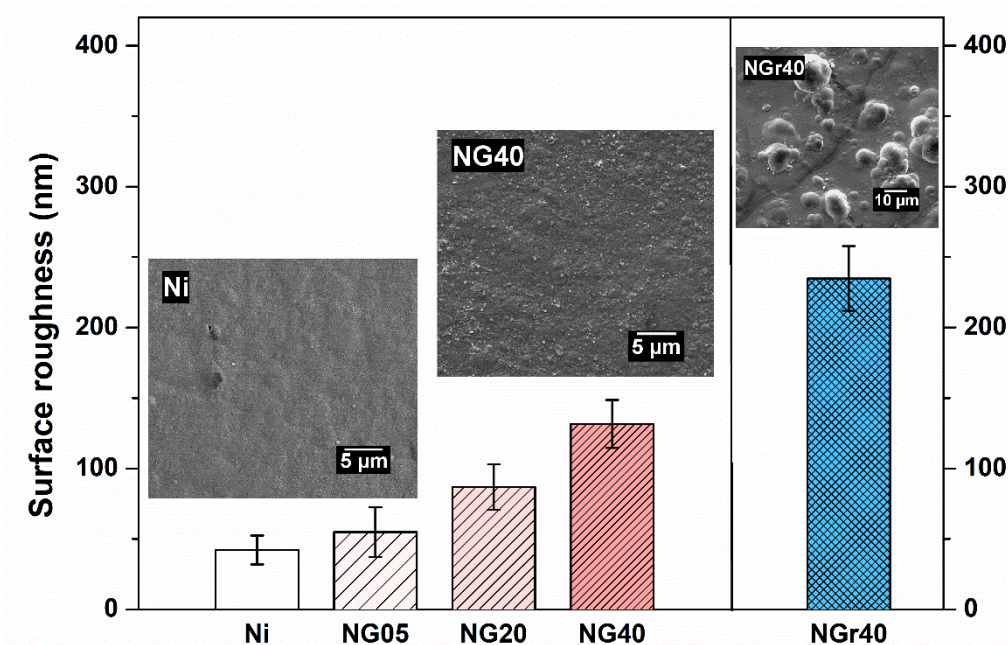
Fig. 1. Surface roughness and morphology of the GO-free Ni coating and those incorporated with GO (NG05, NG20, NG40) or graphite (NGr40).

Fig. 1 compares the surface roughness of the samples. Clearly, the surface roughness of the coating increased with the GO load in the plating solution, and the nickel-graphite composite coating (NGr40) nearly doubled the surface roughness of NG40. SEM images (Fig. 1 inset) showed that the surface of the GO-free nickel coating was relatively compact and smooth, while NG40 was full of fine yet dense nodules due to GO incorporation. Our previous study has revealed that GO sheets were introduced homogeneously not only at the surface but also throughout the depth of the coating, wrapping and intersecting the nickel crystallites, thus causing a grain refinement effect and the rise in mechanical strength as well as surface roughness [27]. In contrast, with the same incorporation mass of 4 mg/ml, the graphite reinforced coating NGr40 showed irregularities in much greater sizes on the surface due to the thickness of the graphite particles inside. The GO-free Ni deposit exhibited a Vickers' hardness of H_v 524±38, close to the values in the literature on nickel coatings by EBP [20, 29]. The hardness was improved gradually as GO was introduced, with the peak value of H_v 680±57 for NG20, which is 31% higher than that of the GO-free coating. NG40 exhibited a slightly reduced hardness compared to NG20, while the

136   hardness of NGr40 was measured to be H_v 574±20.

137   **3.2. Sliding against steel**
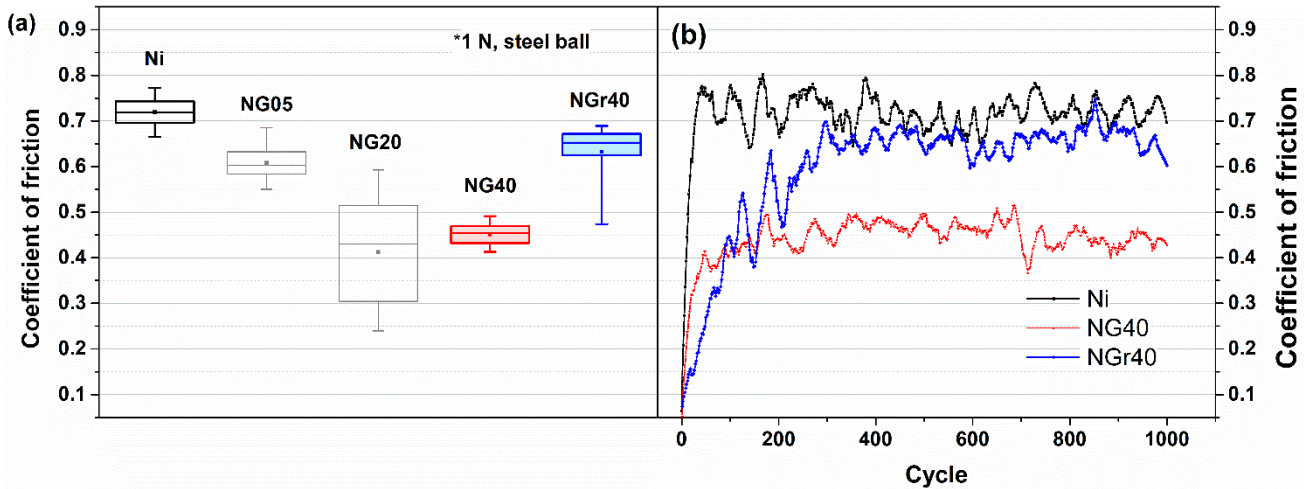
139   Fig. 2. (a) Coefficient of friction box plots of the GO-free Ni and the composite coatings
140   against a chromium bearing steel ball over 1000 cycle reciprocating sliding under a load of
141   1 N. The boxes and whiskers represent the 1st quartiles and the 1st standard deviations,
142   respectively. (b) typical COF curves for Ni, NG40 and NGr40.

143   Fig. 2 presents the frictional behaviour of the coatings during reciprocating tribological
144 tests against a bearing steel ball under a normal load of 1 N. As shown in Fig. 2a, all the
145 four composite coatings exhibited reduced coefficient of friction (COF, μ) compared to the
146 GO-free Ni coating (μ ~0.72). NG20 achieved the lowest possible friction against the steel
147 ball. However, note that its COF spread over a wide range, indicating unstable friction
148 conditions. NG40 showed a substantially lower steady-state μ of ~0.45. It is also worth
149 noting that the three nickel-GO coatings outperformed the nickel-graphite coating NGr40.
150 As shown in Fig. 2b, the COF of the GO-free Ni coating reached a plateau after a short
151 running-in period. NGr40 showed a marginally reduced μ, levelling off at ~0.65. Its
152 prolonged running-in period can be attributed to its high surface roughness which increased
153 the time required for stabilising the contact.

154
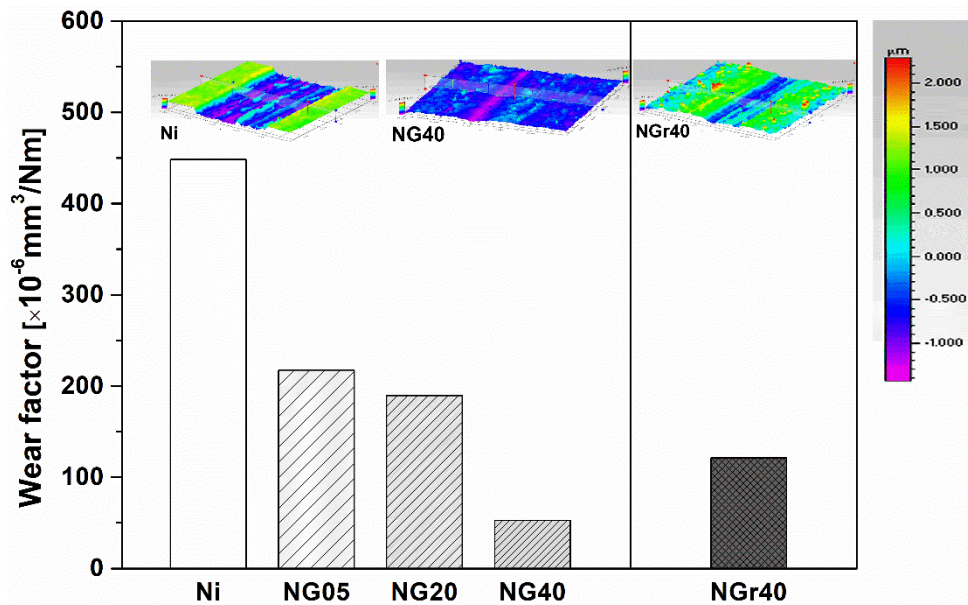
Fig. 3. Wear factors for GO-free Ni, NG05, NG20, NG40 and NGr40 measured after 1000-cycle sliding against a bearing steel ball under a normal load of 1 N. The insets show the 3-dimensional profiles of the worn Ni, NG40 and NGr40. A colour scale bar for the height profiles is attached aside the plot.

The wear factors of the coatings during the tests are summarised in Fig. 3. Compared with the GO-free Ni coating, the wear factors for NG05, NG20 and NG40 were reduced by 51.5%, 58.0% and 88.2%, respectively. The wear factor of NGr40, although clearly lower than that of Ni, was nearly double that of NG40. From the height profiles of the worn coating surfaces as the insets in Fig. 3, it is clear that the wear scar on NG40 is significantly smaller than that on the GO-free Ni coating (60 *vs.* 310 μm in width, and 0.3 *vs.* 2 μm in depth). In comparison, NGr40 achieved a moderate reduction in the wear loss.

As shown in Fig. 4, the GO-free nickel coating after wear showed heavy cutting, furrows and push-ups on the bottom of the wear scar, denoting severe sliding adhesive wear and galling. The large density of fine wear debris present within the wear scar implies that three-body abrasion could also have taken place. EDS analysis (Position 1&2 in Fig. 4b) indicates that the build-ups were high in oxygen while the lower positions of the wear scar showed little oxygen. The information above suggests that the coating surface was oxidised but then destructed into debris during the unlubricated wear. Consequently, severe metal-to-metal rubbing occurred.
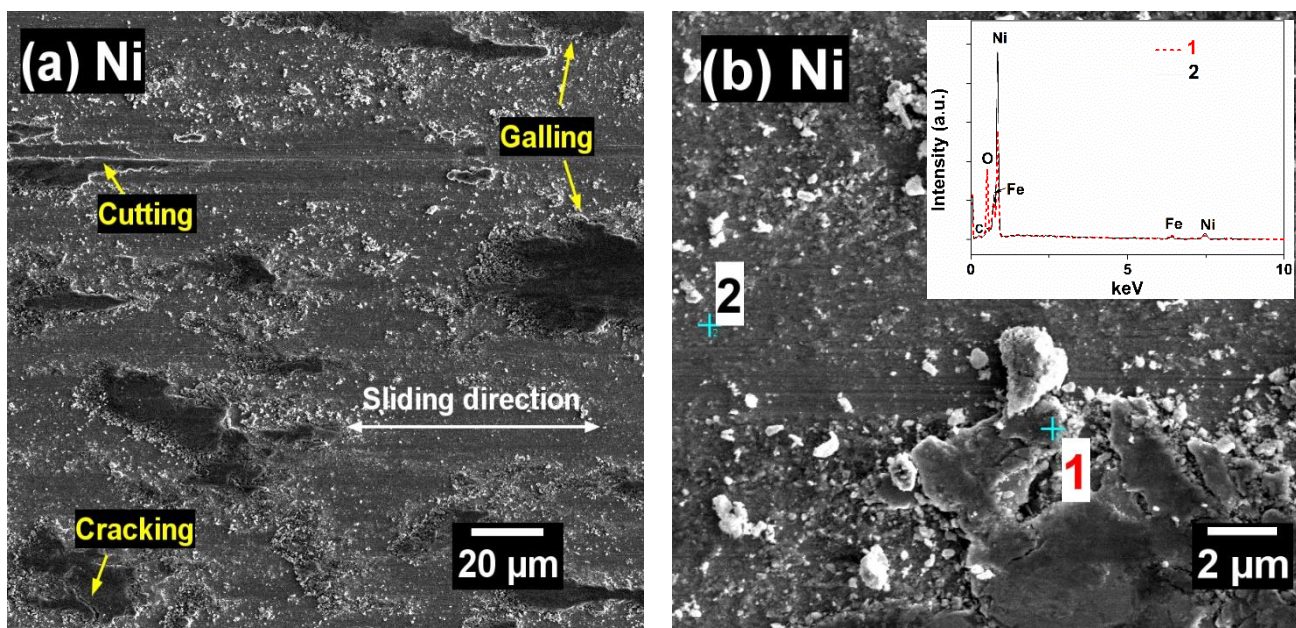
Fig. 4. SEM images and EDS spectra (inset of b) of the worn GO-free Ni coating sliding against a bearing steel ball in air under a load of 1 N.

Figs. 5a-c demonstrate the morphology of the worn NG05, NG20 and NG40. The surface of NG05 was rubbed heavily, presenting similar features due to severe adhesive wear as with the GO-free Ni. Nonetheless, a larger fraction of the wear-induced oxide film was retained (Fig. 5a). NG20 exhibited less coating deformation after wear (Fig. 5b). Substantial reduction in wear was achieved on NG40 which showed only a mild degree of material flow and negligible amount of wear debris (Fig. 5c). The wear track width was reduced from 250 μm for NG05 to 60 μm for NG40. In order to track the structural changes of the incorporated GO during wear, the worn surface of NG40 was inspected by Raman spectroscopy (Fig. 5d). A typical GO spectrum containing a D band around 1350 cm^{-1} and a G band around 1600 cm^{-1} can be obtained from the unworn surface. After wear, attenuated D and G bands, characteristic of GO, were still detectable near the edges of the wear scar (Positions 2 and 3 in Fig. 5c). The Raman D and G bands diminished to minimum around the centre of the wear scar (Position 1 in Fig. 5c). It is likely that the GO sheets had been pushed away from the central zone where the contact stress was the highest and replaced by thick metal oxide grown on site. Nonetheless, more detailed Raman analysis (such as Raman mapping of the G-band and D/G ratio) should be conducted in order to elucidate the structural changes in GO within the wear tracks.
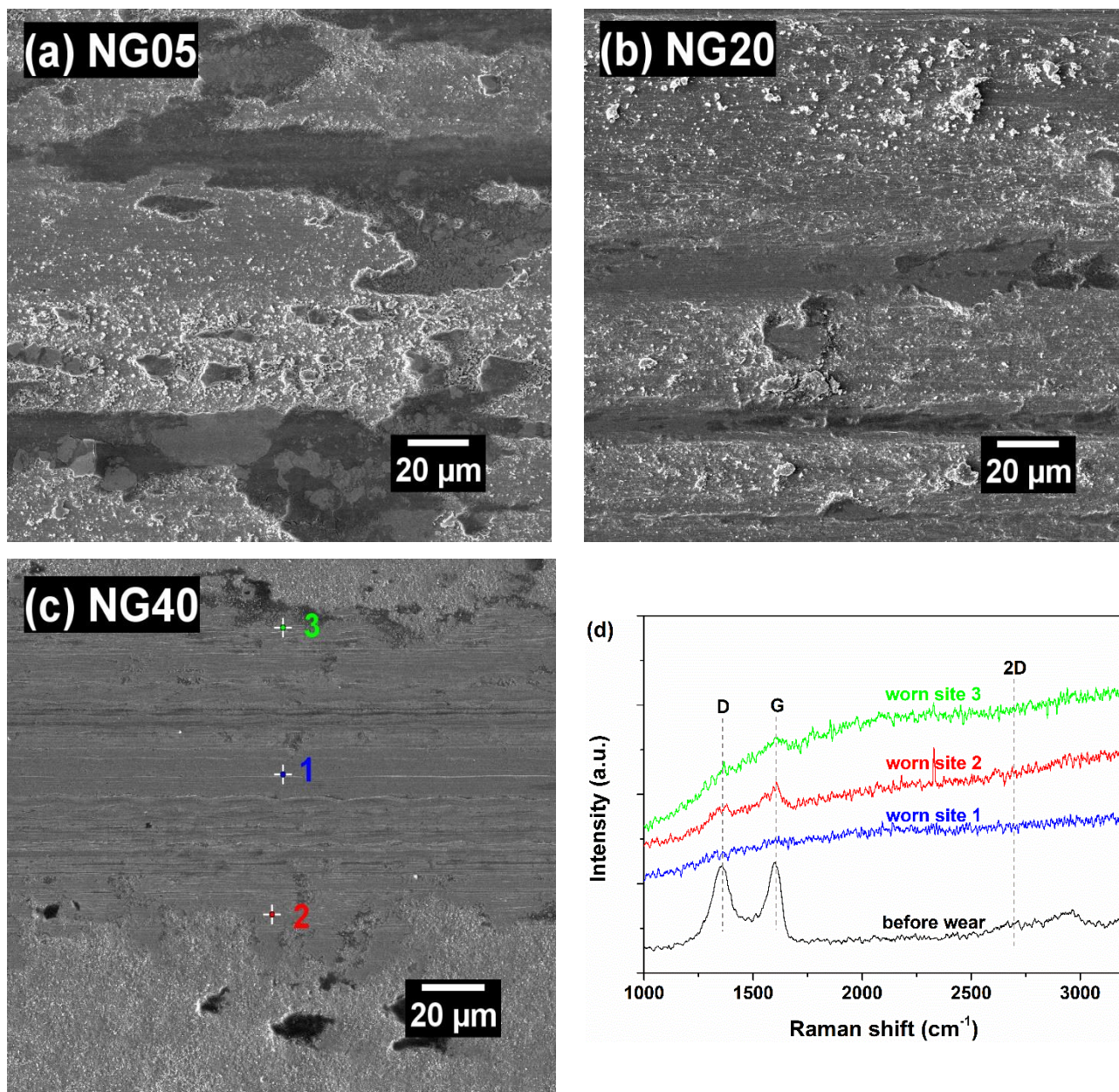
Fig. 5. Worn surfaces of (a) NG05, (b) NG20 and (c) NG40 after sliding against a Cr ball in air under a load of 1 N. (d) Raman spectra obtained from the marked positions in (c).

The worn NGr40 (Fig. S1, Supplementary document) resembled the worn GO-free nickel coating. Back-scattered electron microscopy and EDS mapping indicate a discontinuous oxide film on the worn NGr40, likely due to the insufficient lubricating effect by the graphite fillers, which led to severe plastic flow at the sliding contact as previously seen on the GO-free Ni coating.
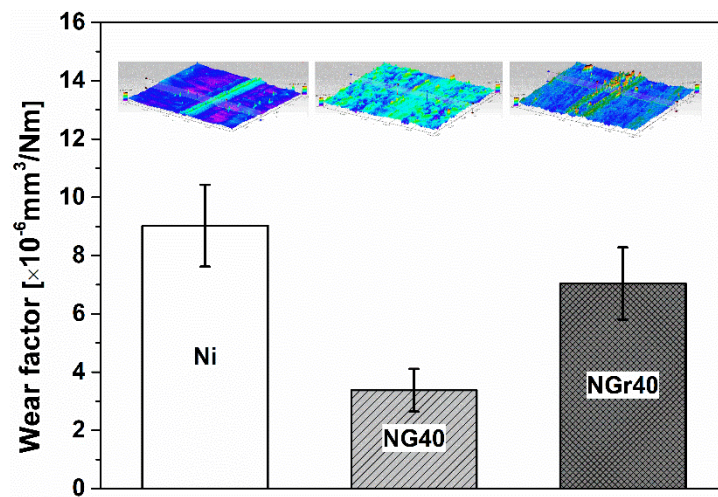
3.3. Sliding against alumina
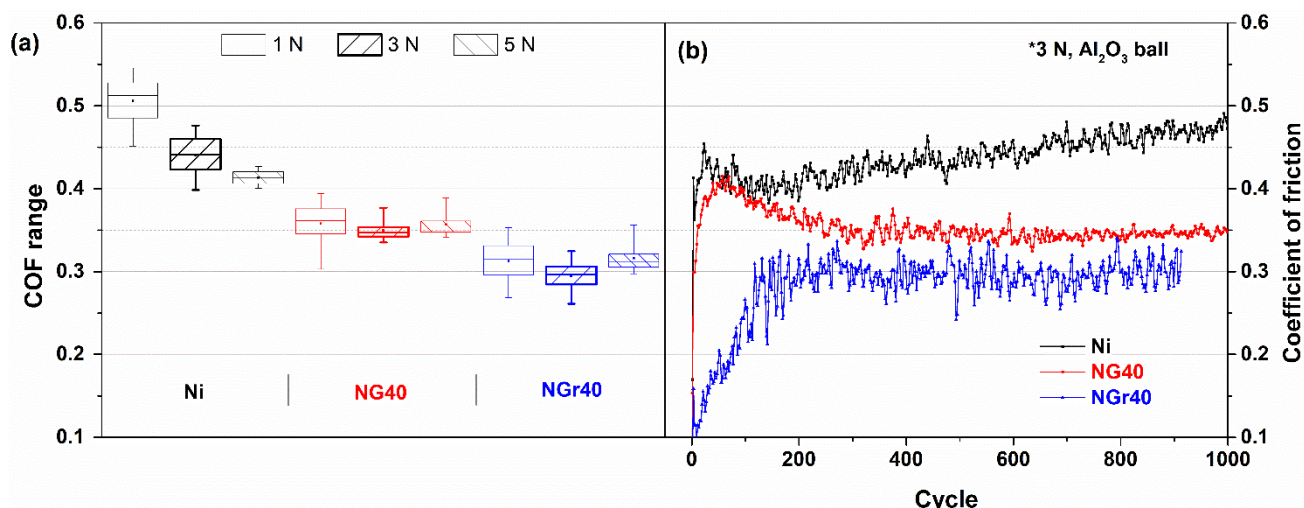
Fig. 6. (a) Coefficient of friction box plots of Ni, NG40 and NGr40 against an alumina ball under varying normal loads. (b) typical COF curves under a load of 3 N.

Fig. 6 shows the friction behaviour of Ni, NG40 and NGr40 against the alumina ball under varying loads. Due to reduced metallurgical compatibility between the ceramic and metallic coating tribo-pairs, all the samples exhibited lower friction against alumina than against steel as seen in Fig. 2. Under 3 N, the COF of the GO-free Ni increased progressively over cycles, denoting a changing sliding contact. NG40 showed a steady-state COF of 0.35 after a quick running-in stage. The COF of NGr40 was lower than NG40, reaching a steady-state value of 0.3, likely due to the high surface roughness of NGr40 (see Fig. 1) and the solid lubricating effect of graphite particles.

The wear tracks were then scanned by a 3D profilometer, and the wear factors calculated, as summarised in Fig. 7. Close inspection of the wear scar formed on the GO-free Ni coating revealed abrasion-induced grooves and push-ups. The wear scar on NGr40 was slightly smaller yet irregular. For NG40, no appreciable material loss but just a flattening effect was found on the tested site. Accordingly, the wear factor for the GO-free Ni coating was the largest (9×10^{-6} $mm^3N^{-1}m^{-1}$). It decreased by about 60% for NG40, indicating significantly enhanced wear resistance. Although NGr40 exhibited slightly lower COF than NG40 (Fig. 6), its wear factor was found to be much higher than NG40.

Fig. 7. Wear factors for GO-free Ni, NG40 and NGr40 sliding in air against an alumina ball under a normal load of 3 N.

Fig. 8 compares the detailed morphology of the coatings worn against the alumina counterface. The worn Ni coating (Fig. 8a) showed a wavy topography, predominated by detached, stripe-like tribo-films due to lack of lubrication. EDS analysis indicates that while the lower positions showed the coating composition with little oxygen signal, the tribo-films were high in carbon and oxygen. The worn NGr40 (Fig. 8b) showed cracks and spallation. The original surface lumps due to the underneath graphite particles were flattened by the slider and the wear debris was accommodated between these surface fluctuations (Fig. S2, Supplementary document), which could have contributed to the lower COF of NGr40 as shown in Fig. 6.

The wear scar on NG40 (Fig. 8c) appeared to be smooth with very fine grooves, indicating mild abrasive wear. EDS element mapping (Fig. 8d) showed that oxygen was homogeneously present over the worn zone, indicating a continuous oxide film formed on NG40. Within the centre zone of the wear scar, signs of minor material flow along the sliding direction were observed as shown in Fig. 8e. Around the edge of the wear track exist translucent carbon-rich scales, as shown in Fig. 8f, which are very likely solid lubricant films formed of worn GO sheets.
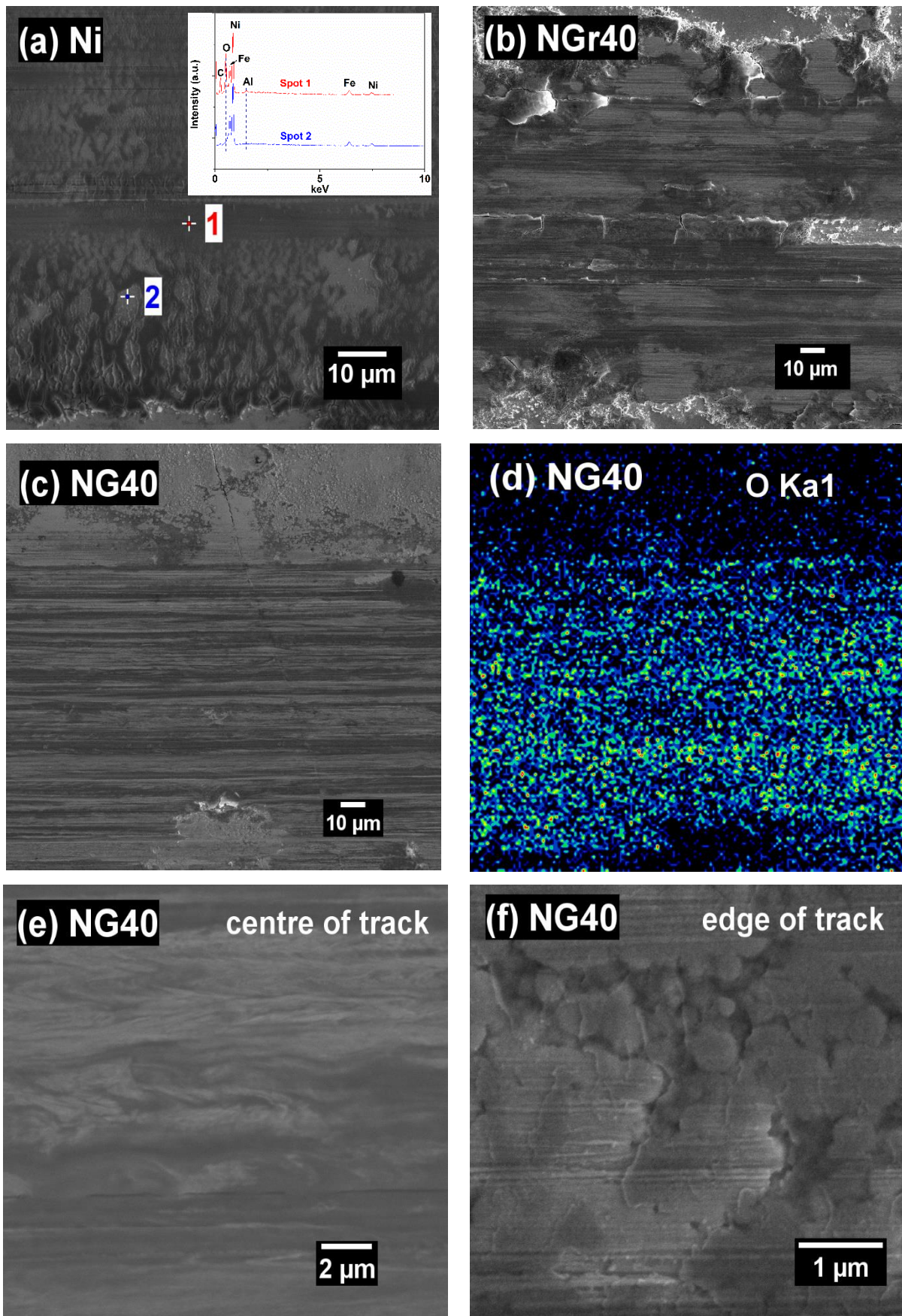
Fig. 8. Worn surface of (a) GO-free Ni, (b) NGr40 and (c-f) NG40 sliding against alumina under a load of 3 N.

4. Discussion

4.1. Effect of GO

In this research, GO was found effective in suppressing friction and improving wear resistance of the nickel matrix. The most pronounced improvement, for instance, was observed for the NG40-steel tribo-pair, whose COF and wear factor were about 37% and 88% lower than the Ni-steel tribo-pair, respectively.

The reasons for the reduction in friction coefficient and wear could be three-fold. Firstly, it can be ascribed to the increased hardness (H) and the reduced plasticity. According to the adhesive theory of wear [30], the coefficient of friction μ between a tribo-pair, formed of a rigid counterpart and an engineering surface in multi-asperity contact, can be expressed by the following equation:

$$\mu_{adh} = \frac{F}{W} = \frac{\tau}{\sqrt{\sigma^2 - a\tau^2}} \approx \frac{\tau_i}{\sigma} \tag{2}$$

where F is the tangential frictional force, W is the normal load, τ is the shear strength of the bulk material, σ is the corresponding compression yield strength, and a is a numerical factor, determined empirically. The equation receives a simplified form as shown at its right end when the surface is covered by a weak interfacial film of low shear strength τ_i, such as oxide scale grown in-situ. It is therefore clear that a lower μ_{adh} could be obtained if the yield strength σ, which is proportional to the indentation hardness of the bulk, is improved.

Hardness is also known to affect the resistance to abrasive wear inversely. Indeed, the COF evolution (Fig. 2) of the composite coatings NG05, NG20 and NG40 exhibited good compliance to their hardness values; the COFs were reduced to an extent comparable to the degree of their hardness improvement.
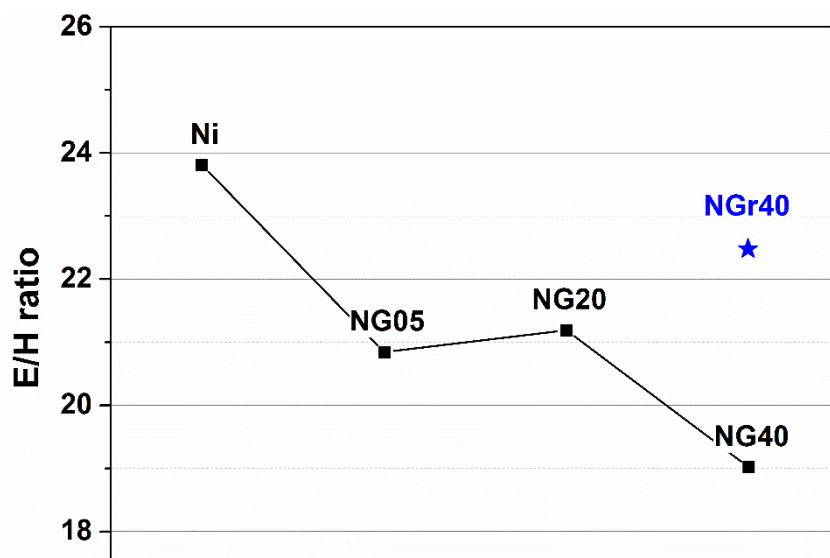
Fig. 9 E/H ratio of the coating as a function of GO/graphite incorporation.

The ratio between Young's (elastic) modulus and hardness E/H, which is indicative of the plasticity of a material, can play a significant role in the tribological performance [31, 32]. A lower E/H ratio means that the material is less prone to plastic deformation, i.e., the contact between sliding asperities is more elastic. Consequently, the energy dissipation, which is responsible for friction, can be mitigated. In addition, according to Bowden and Tabor's [30] adhesive wear mode, reduced plasticity can effectively reduce cold weld and growth of junction, thus leading to reduced adhesive wear. The E/H ratio values for the GO-free Ni and the Ni-GO composite coatings in this work were calculated from nanoindentation measurements and plotted in Fig. 9. It shows that the E/H ratio values were reduced effectively after introducing GO into the matrixes. Particularly, NG40 showed an E/H ratio of 18.6, which is significantly lower than that (23.8) of the GO-free Ni coating. This is in agreement with its wear factor which is the smallest among all the samples (Fig. 3).

Secondly, the improved tribological performance of Ni-GO composite coatings is also owing to the formation of a continuous easy-shear oxide film on the coating surface. As can be seen in Fig. 4, the worn GO-free Ni coating showed material 'islands' across the wear track, which were the oxides of the metallic coating. It is known that oxide films, formed naturally on metals in air, are of much significance in determining the tribological behaviour, as the oxides can serve as a low shear strength film which reduces the μ of the tribo-pair (refer to Equation 2). However, if the oxide film is incomplete or penetrated by the slider, high friction is very likely, due to direct metallic contact, and so the wear factor, as in the case of the GO-free Ni. The formation of such an incomplete oxide film was also observed on the worn NGr40 which incorporates graphite flakes (Fig. S1), which could be the reason for its marginally lowered friction and wear. In contrast, the worn Ni-GO composite coatings have showed decreasing amount of surface irregularities as the GO content increased (Fig. 5), which implies a better retention of the surface oxides. The enhanced retention of the oxide films is likely due to the reduced plasticity of the bulk coatings as discussed, and can also be related to the lubricating GO sheets which mitigated the tangential frictional force applied to the surface metallic oxide. As a result, the adhesion and plastic flow during sliding were suppressed, and the wear mechanism changed gradually from plasticity-dominated for GO-free Ni (severe adhesive wear) to oxidation-dominated for NG40 (mild oxidation wear).

Last but not least, the lubricating effect of GO should be appreciated, too. Graphene and its derivatives (including GO) have been reported to be promising novel solid lubricants [33]. With regards to graphene-containing composites, it has been reported that a carbon-

301 rich transfer layer can be formed on top of the sliding composite surface [25]. This carbon-
302 rich transfer layer can further contribute to a lower τ_i in Equation 2, thus lubricating the
303 sliding. Indeed, Raman spectroscopy showed residues of the features of GO in the edge
304 zone of the wear track (Fig. 5). The features were gone at the centre of the wear scar,
305 suggesting that the GO sheets at such places may have been transformed into amorphous
306 carbon, if not a complete removal.

307 More interestingly, apart from the Raman analysis results, nano-sized GO rolls were
308 also observed existing within the worn scar, as demonstrated in Fig. 10. The sectioning of
309 the GO rolls using focused ion beam (FIB) revealed the hollow structure of the GO rolls
310 (Figs. 10c-d).
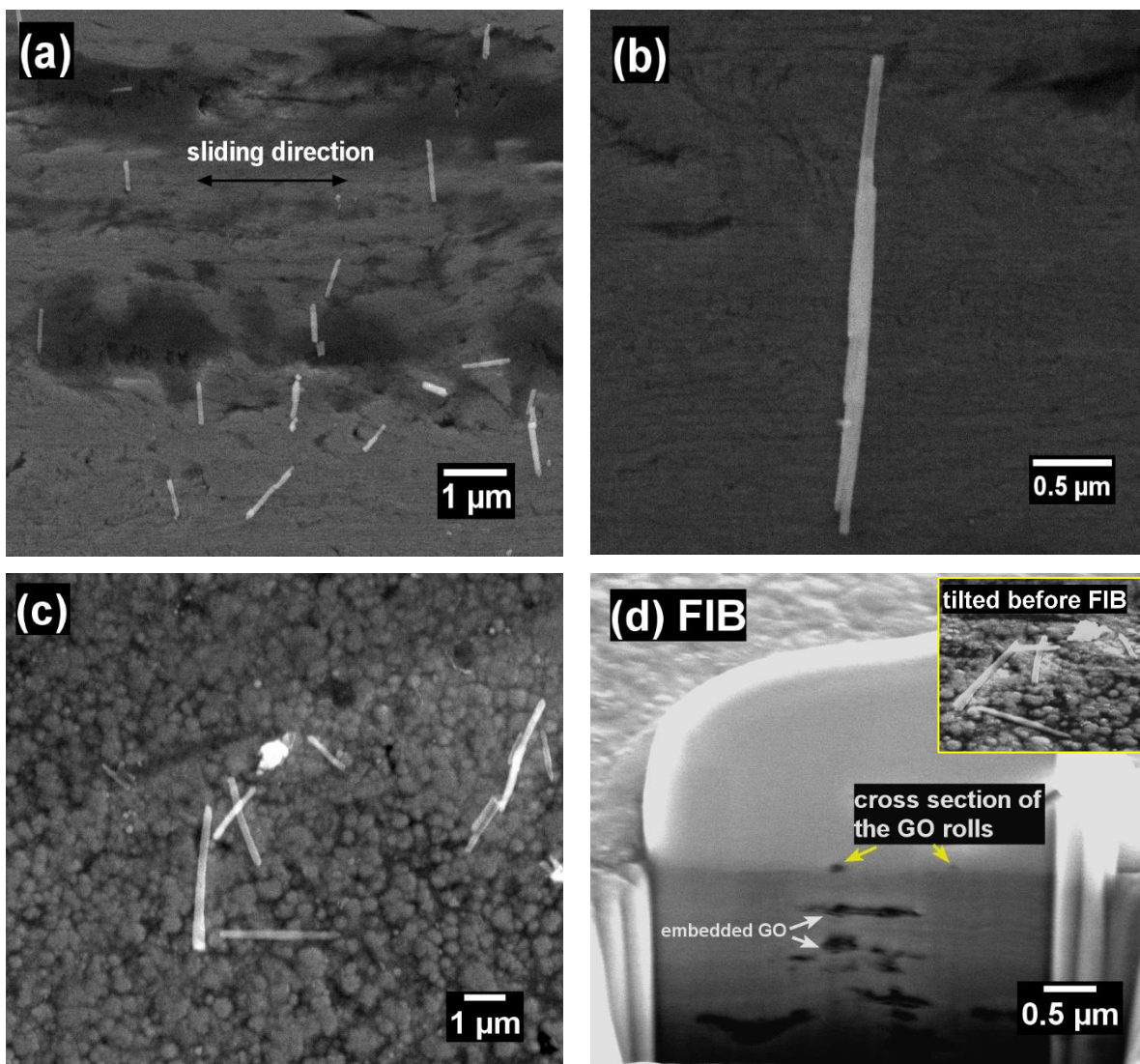
311 Fig. 10 GO rolls formed within the wear track during sliding.

312 Berman et al. [5] report the formation and macroscale superlubricity of graphene
313 nanoscrolls in the presence of nano-diamond particles which could be the first of this kind.
314 Recently, graphene nanoscrolls were found to form on the surface of an amorphous carbon

film during sliding which is responsible for the friction drop [34]. A few other rolling-up carbon structures, such as crumpled graphene balls [35], carbon nano-horns [36], have also been reported to improve the tribology of the sliding surface underneath. However, to our awareness, this is the first report on the observed formation of such graphene nanorolls from not a single layer graphene coating or graphene-based lubricants, but a graphene-based composite during sliding contact.

As can be seen in Fig. 10, the GO nanorolls were uniform in diameter and distributed mostly perpendicular to the sliding direction. The formation could therefore be attributed to the generation of structural defects on the upside of the GO sheets during sliding in conjunction with the dragging force of the slider [5]. The friction-reduction mechanisms that have previously been suggested for these rolling graphene structures include nano ball bearing, sliding and exfoliation [34, 36]. In view of the high contact pressure (500-1000 MPa) applied in this work which may squeeze and permanently deform the hollow GO rolls once upon formation, the nano bearing effect is unlikely to take place (Indeed, the GO rolls were mainly found close the edges of the wear scar, while few GO rolls were observed at the centre where the contact pressure was high). Rather, the sliding mechanism, in which the GO nanorolls acted as separators of low surface energy between the tribo-pair, is more plausible. Moreover, GO sheets are so thin and flexible that a fraction of the sliding motion energy can be easily dissipated by means of nanoroll formation, hence leaving less energy that is converted into friction.

### 4.2. Effect of counter material

Fig. 11 compares the bearing steel counterface after wear against the GO-free Ni and the NG40 coatings. The size of the wear track on the steel counter ball against NG40 was remarkably smaller than that against Ni. In the meantime, although subject to the same cleaning process after the wear test, the counter ball against the Ni coating showed a greater amount of nickel adhesion as proved by EDS mapping. This is due to high metallurgical compatibility for the metal-to-metal tribo-pair. The cold-welded asperities between the two surfaces were then fractured over time, eventually leading to failure of the tribo-film. This explains the high COF and wear factor of the GO-free Ni coating. The reduced Ni attachment on the counter ball against NG40 could be attributed to the GO sheets within the composite coating which inhibited direct metal-to-metal contact during the wear test.
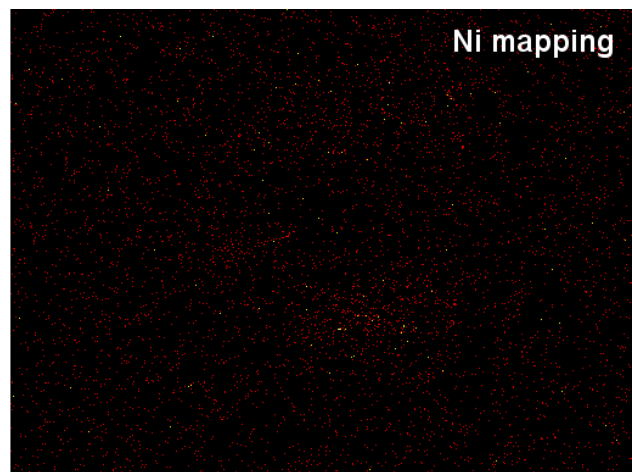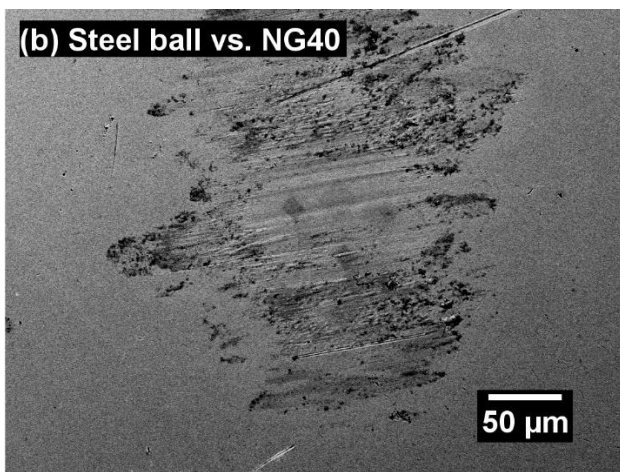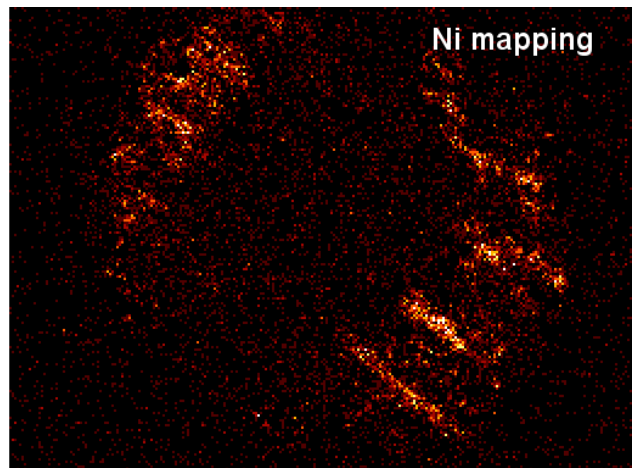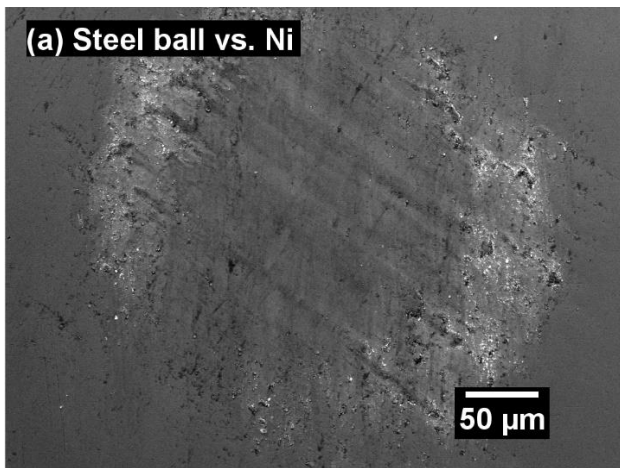
Fig. 11. The bearing steel counter balls after wear against (a) Ni and (b) NG40.
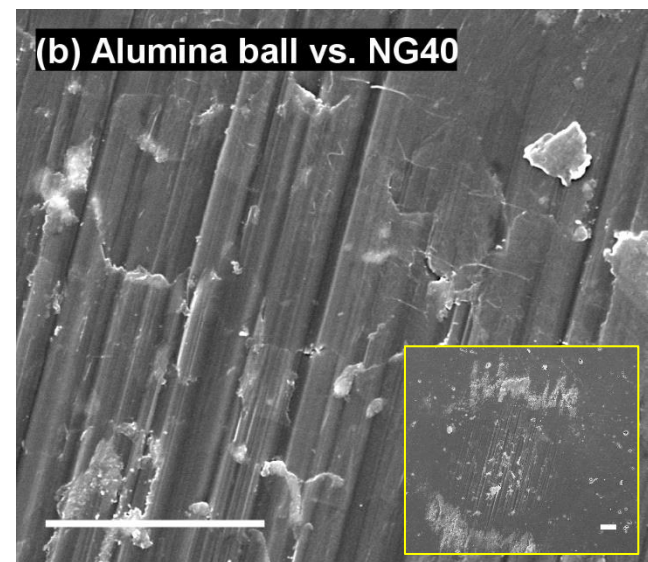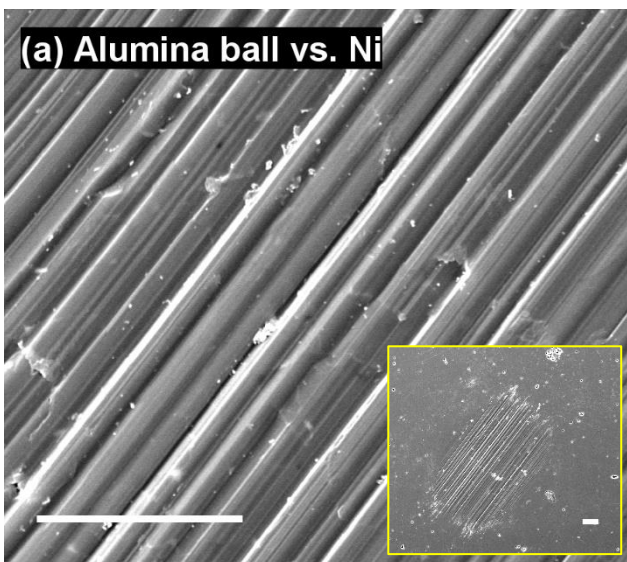
Fig. 12. The alumina counter balls after wear against (a) Ni and (b) NG40. Scale bars 20 μm.

Fig. 12 shows the wear on the ceramic counter balls against the same coatings. No appreciable Ni adhesion was detected by EDS in both cases, which explains the lower

353 friction and wear of the coatings compared with those against steel. The ball against Ni
354 exhibited deep and clear grooves. In comparison, the wear grooves on the counter ball
355 against NG40 appeared to be much shallower, suggesting less abrasion during the test.
356 This can be attributed to the transfer film formed on the counter ball (as seen in Fig. 12b)
357 which lubricated the sliding.

4.4. Wear mechanisms for GO and graphite reinforced composites

In the present study, a nickel-graphite composite coating was purposely designed and tested for comparison. Based on the results and discussion above, different wear mechanisms for graphene-metal composite coatings and graphite-metal composite coatings are proposed, as illustrated in Fig. 13. Owing to the extremely thin nature of graphene, the composite incorporating GO (or other graphene derivatives), given that the graphene-based fillers are homogeneously distributed (Fig. 13a), is a nano-structured material, which is free of surface lumps observed on its graphite counterpart (Fig. 13d).

During sliding wear, a continuous metallic oxide film, which is favourable for lower friction and wear, can be retained on the surface of the GO-reinforced composite coating, due to the pinning and strengthening effects of GO (Fig. 13b). As the sliding continues, not only the metallic oxide layer gets thicker, an extra thin lubricating film comprising of squeezed GO sheets is also formed on top (Fig. 13c). Meanwhile, there are chances that GO sheets are peeled off by the slider and form nanorolls (see Fig. 10) which reduce the surface energy and thus the friction.

The graphite-reinforced composite coating, by contrast, achieves low friction mainly by the smearing of graphite flakes (Fig. 13e). Given the limited availability of graphite sites on the surface, discrete metallic oxide islands instead of a continuous oxide film are formed, and a large amount of wear debris occurs. Meanwhile, the uneven distribution of stress between the graphite-containing lumps and the squeezed wear debris can lead to cracks and spallation (Fig. 13f).

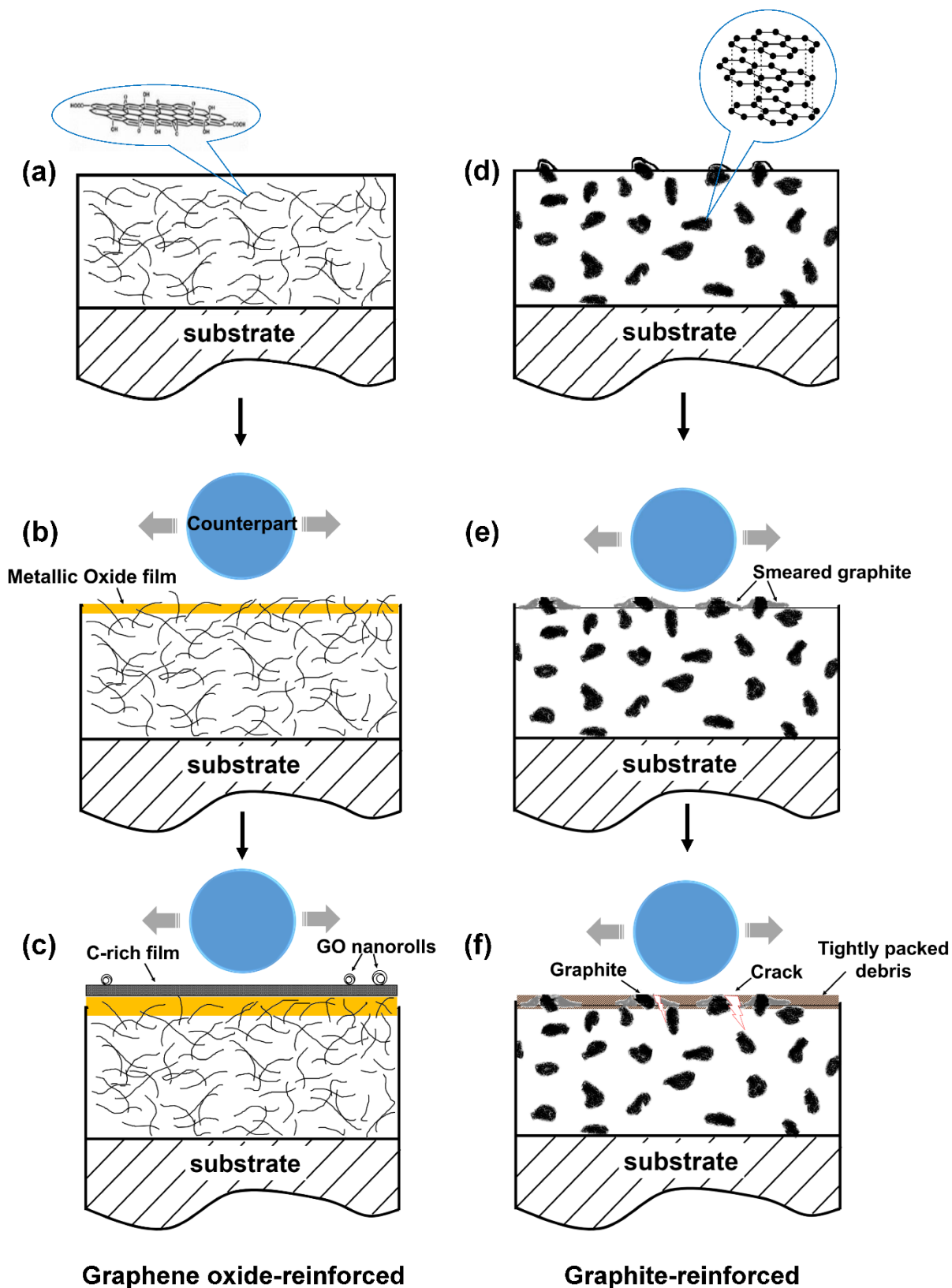**Graphene oxide-reinforced**

Graphite-reinforced

380

381 Fig. 13 Illustrations of the different wear mechanisms for (a-c) graphene-metal and (d-f)

382 graphite-metal composites.

383

384

5. Conclusions

In this study, the tribological behaviour of electro-brush plated Ni, Ni-GO and Ni-graphite composite coatings against steel and ceramic was compared. It was found that the incorporation of GO can effectively suppress the friction of the GO-free nickel coating (up to 47% less against a bearing steel ball, and 30% less against an alumina ball). As the GO load increases from 0 to 4 mg/ml, the wear rate of the resulting composite can be reduced significantly by approximately 90%. The lubrication and wear mechanisms of the composite coatings were studies by EDS, Raman, FIB and nanoindentation, which suggest the effects of GO as mechanical strengthening, reducing the adhesion between the tribo-pair and promoting the retention of oxide tribo-film on the coating. Interestingly, close microscope examination showed sliding-induced GO rolls in the wear tracks, suggesting an additional lubricating effect. The incorporation of graphite particles can also improve the tribological performance of the coating by the lubricating effect of graphite, but the improvement is limited compared to those with GO due to the size and distribution effect of the graphite incorporations.

Acknowledgements

References

[1] O. Penkov, H.-J. Kim, H.-J. Kim, D.-E. Kim, Tribology of graphene: A review, Int. J. Precis. Eng. Man., 15 (2014) 577-585.

[2] C. Lee, X. Wei, Q. Li, R. Carpick, J.W. Kysar, J. Hone, Elastic and frictional properties of graphene, Phys. Status Solidi B, 246 (2009) 2562-2567.

[3] K.S. Kim, H.J. Lee, C. Lee, S.K. Lee, H. Jang, J.H. Ahn, J.H. Kim, H.J. Lee, Chemical vapor deposition-grown graphene: the thinnest solid lubricant, ACS nano, 5 (2011) 5107-5114.

[4] D. Marchetto, C. Held, F. Hausen, F. Wählisch, M. Dienwiebel, R. Bennewitz, Friction and wear on single-layer epitaxial graphene in multi-asperity contacts, Tribol. Lett., 48 (2012) 77-82.

[5] D. Berman, S.A. Deshmukh, S.K.R.S. Sankaranarayanan, A. Erdemir, A.V. Sumant, Macroscale superlubricity enabled by graphene nanoscroll formation, Science, 348 (2015) 1118-1122.

[6] S. Stankovich, D.A. Dikin, G.H. Dommett, K.A. Kohlhaas, E.J. Zimney, E.A. Stach, R.D. Piner, S.T. Nguyen, R.S. Ruoff, Graphene-based composite materials, Nature, 442 (2006) 282-286.

[7] Y. Liu, Z. Dang, Y. Wang, J. Huang, H. Li, Hydroxyapatite/graphene-nanosheet composite coatings deposited by vacuum cold spraying for biomedical applications: Inherited nanostructures and enhanced properties, Carbon, 67 (2014) 250-259.

[8] A. Dorri Moghadam, E. Omrani, P.L. Menezes, P.K. Rohatgi, Mechanical and tribological properties of self-lubricating metal matrix nanocomposites reinforced by carbon nanotubes (CNTs) and graphene – A review, Compos. Part B Eng., 77 (2015) 402-420.

[9] C. Min, P. Nie, H.-J. Song, Z. Zhang, K. Zhao, Study of tribological properties of polyimide/graphene oxide nanocomposite films under seawater-lubricated condition, Tribol. Int., 80 (2014) 131-140.

[10] Z. Xu, L. Chen, X. Shi, Q. Zhang, A.M.M. Ibrahim, W. Zhai, J. Yao, Q. Zhu, Y. Xiao, Formation of friction layers in graphene-reinforced TiAl matrix self-lubricating composites, Tribol. Trans., 58 (2015) 668-678.

[11] Y. Meng, F. Su, Y. Chen, Synthesis of nano-Cu/graphene oxide composites by supercritical CO2-assisted deposition as a novel material for reducing friction and wear, Chem. Eng. J., 281 (2015) 11-19.

[12] F. Chen, J. Ying, Y. Wang, S. Du, Z. Liu, Q. Huang, Effects of graphene content on the microstructure and properties of copper matrix composites, Carbon, 96 (2016) 836-842.

[13] D. Kuang, L. Xu, L. Liu, W. Hu, Y. Wu, Graphene–nickel composites, Appl. Surf. Sci., 273 (2013) 484-490.

[14] H. Algul, M. Tokur, S. Ozcan, M. Uysal, T. Cetinkaya, H. Akbulut, A. Alp, The effect of graphene content and sliding speed on the wear mechanism of nickel–graphene nanocomposites, Appl. Surf. Sci., 359 (2015) 340-348.

[15] B. Xu, H. Wang, S. Dong, B. Jiang, Fretting wear-resistance of Ni-base electro-brush plating coating reinforced by nano-alumina grains, Mater. Lett., 60 (2006) 710-713.

[16] C.K. Lee, Wear and corrosion behavior of electrodeposited nickel–carbon nanotube composite coatings on Ti–6Al–4V alloy in Hanks′ solution, Tribol. Int., 55 (2012) 7-14.

[17] Z. Ren, N. Meng, K. Shehzad, Y. Xu, S. Qu, B. Yu, J.K. Luo, Mechanical properties of nickel-graphene composites synthesized by electrochemical deposition, Nanotechnology, 26 (2015) 065706-065711.

[18] C. Guo, Y. Zuo, X. Zhao, J. Zhao, J. Xiong, Effects of surfactants on electrodeposition of nickel-carbon nanotubes composite coatings, Surf. Coat. Tech., 202 (2008) 3385-3390.

[19] J. Sudagar, J. Lian, W. Sha, Electroless nickel, alloy, composite and nano coatings – A critical review, J. Alloy. Compd., 571 (2013) 183-204.

[20] B. Jiang, B. Xu, S. Dong, Y. Yi, P. Ding, Contact fatigue behavior of nano-ZrO2/Ni coating prepared by electro-brush plating, Surf. Coat. Tech., 202 (2007) 447-452.

[21] C.-D. Gu, J.-L. Zhang, W.-Q. Bai, Y.-Y. Tong, X.-L. Wang, J.-P. Tu, Electro-Brush Plating from Deep Eutectic Solvent: A Case of Nanocrystalline Ni Coatings with Superior Mechanical Property and Corrosion Resistance, J. Electrochem. Soc., 162 (2015) D159-D165.

[22] W. Zhai, X. Shi, M. Wang, Z. Xu, J. Yao, S. Song, Y. Wang, Grain refinement: A

mechanism for graphene nanoplatelets to reduce friction and wear of Ni3Al matrix self-lubricating composites, Wear, 310 (2014) 33-40.

[23] W. Zhai, N. Srikanth, L.B. Kong, K. Zhou, Carbon nanomaterials in tribology, Carbon, 119 (2017) 150-171.

[24] Z. Xu, X. Shi, W. Zhai, J. Yao, S. Song, Q. Zhang, Preparation and tribological properties of TiAl matrix composites reinforced by multilayer graphene, Carbon, 67 (2014) 168-177.

[25] H. Li, Y. Xie, K. Li, L. Huang, S. Huang, B. Zhao, X. Zheng, Microstructure and wear behavior of graphene nanosheets-reinforced zirconia coating, Ceram. Int., 40 (2014) 12821-12829.

[26] Y. Meng, F. Su, Y. Chen, A novel nanomaterial of graphene oxide dotted with Ni nanoparticles produced by supercritical CO_2-assisted deposition for reducing friction and wear, ACS applied materials & interfaces, 7 (2015) 11604-11612.

[27] S. Qi, X. Li, Z. Zhang, H. Dong, Fabrication and characterisation of electro-brush plated nickel-graphene oxide nano-composite coatings, Thin Solid Films, 644 (2017) 106-114.

[28] W.C. Oliver, G.M. Pharr, An improved technique for determining hardness and elastic modulus using load and displacement sensing indentation experiments, J. Mat. Res., 7 (1992) 1564-1583.

[29] Z. Li, S. Qian, W. Wang, H. Shen, H. Long, High-temperature tribological properties of Ni-P alloy coatings deposited by electro-brush plating, Rare Met., 30 (2011) 669-675.

[30] I.M. Hutchings, Tribology: friction and wear of engineering materials, Edward Arnold, London, 1992.

[31] H. Dong, T. Bell, Enhanced wear resistance of titanium surfaces by a new thermal oxidation treatment, Wear, 238 (2000) 131-137.

[32] A. Leyland, A. Matthews, On the significance of the H/E ratio in wear control: a nanocomposite coating approach to optimised tribological behaviour, Wear, 246 (2000) 1-11.

[33] D. Berman, A. Erdemir, A.V. Sumant, Graphene: a new emerging lubricant, Mater. Today, 17 (2014) 31-42.

490   [34] Z. Gong, J. Shi, B. Zhang, J. Zhang, Graphene nano scrolls responding to superlow
491   friction of amorphous carbon, Carbon, 116 (2017) 310-317.

492   [35] X. Dou, A.R. Koltonow, X. He, H.D. Jang, Q. Wang, Y.-W. Chung, J. Huang, Self-
493   dispersed crumpled graphene balls in oil for friction and wear reduction, PNAS, 113 (2016)
494   1528-1533.

495   [36] V. Zin, S. Barison, F. Agresti, L. Colla, C. Pagura, M. Fabrizio, Improved tribological and
496   thermal properties of lubricants by graphene based nano-additives, RSC Adv., 6 (2016)
497   59477-59486.

498